

Research Report: Regular Manuscript

Hippocampal representation of threat features and behavior in a human approach-avoidance conflict anxiety task

<https://doi.org/10.1523/JNEUROSCI.2732-19.2020>

Cite as: J. Neurosci 2020; 10.1523/JNEUROSCI.2732-19.2020

Received: 14 November 2019

Revised: 15 June 2020

Accepted: 20 June 2020

This Early Release article has been peer-reviewed and accepted, but has not been through the composition and copyediting processes. The final version may differ slightly in style or formatting and will contain links to any extended data.

Alerts: Sign up at www.jneurosci.org/alerts to receive customized email alerts when the fully formatted version of this article is published.

Copyright © 2020 Abivardi et al.

This is an open-access article distributed under the terms of the Creative Commons Attribution 4.0 International license, which permits unrestricted use, distribution and reproduction in any medium provided that the original work is properly attributed.

1 **Title:** Hippocampal representation of threat features and behavior in a human
2 approach-avoidance conflict anxiety task

3

4 **Abbreviated title:** Hippocampal Representation of Threat and Behavior

5 **Author names:** Aslan Abivardi*^{1,2}, Saurabh Khemka*^{1,2}, and Dominik R. Bach^{1,2,3}

6 * Equal contribution

7

8 **Affiliations:** ¹Computational Psychiatry Research, Department of Psychiatry, Psychotherapy
9 and Psychosomatics, Psychiatric Hospital, University of Zurich, Zurich, 8032, Switzerland,
10 ²Neuroscience Center Zurich, University of Zurich, Zurich, 8057, Switzerland, ³ Wellcome
11 Centre for Human Neuroimaging and Max Planck UCL Centre for Computational Psychiatry
12 and Ageing Research, University College London, London, WC1N 3BG, United Kingdom.

13

14 **Corresponding author:**

15 Aslan Abivardi M.D.

16 Department of Psychiatry, Psychotherapy and Psychosomatics,

17 Psychiatric Hospital, University of Zurich

18 8032 Zurich, Switzerland

19 aslan.abivardi@puk.zh.ch

20

21 **Number of pages:** 24

22 **Number of figures / tables:** 4 / 5

23 **Number of words for Abstract / Introduction / Discussion:** 250 / 637/ 1500

24

25 **Conflict of Interest:** The authors declare no competing financial interests.

26

27 **Acknowledgements:** AA is supported by Wilhelm-Hurka Foundation (3389322) and EMDO
28 Foundation (1045). DRB is supported by funding from the European Research Council
29 (ERC) under the European Union's Horizon 2020 research and innovation programme (Grant
30 agreement No. ERC-2018 CoG-816564 ActionContraThreat). The Wellcome Trust Centre for
31 Human Neuroimaging is supported by core funding from the Wellcome Trust
32 [203147/Z/16/Z].

33 **Abstract**

34 Decisions under threat are crucial to survival and require integration of distinct situational
35 features such as threat probability and magnitude. Recent evidence from human lesion and
36 neuroimaging studies implicated anterior hippocampus (aHC) and amygdala in
37 approach/avoidance decisions under threat, and linked their integrity to cautious behavior.
38 Here we sought to elucidate how threat dimensions and behavior are represented in these
39 structures.

40

41 Twenty human participants (11 female) completed an approach-avoidance conflict task
42 during high-resolution functional MRI. Participants could gather tokens under threat of
43 capture by a virtual predator, which would lead to token loss. Threat probability (predator
44 wake-up rate) and magnitude (amount of token loss) varied on each trial. To disentangle
45 effects of threat features, and ensuing behavior, we performed a multifold parametric
46 analysis.

47

48 We found that high threat probability and magnitude related to BOLD signal in left anterior
49 hippocampus/entorhinal cortex. However BOLD signal in this region was better explained by
50 avoidance behavior than by these threat features. A priori region-of-interest analysis
51 confirmed the relation of anterior hippocampus BOLD response with avoidance. Exploratory
52 subfield analysis revealed that this relation was specific to anterior CA2/3 but not CA1. Left
53 lateral amygdala responded to low and high, but not intermediate threat probability.

54 Our results suggest that anterior hippocampus BOLD signal is better explained by avoidance
55 behavior than by threat features in approach-avoidance conflict. Rather than representing
56 threat features in a monotonic manner, it appears that anterior hippocampus may compute
57 approach/avoidance decisions based on integration of situational threat features represented
58 in other neural structures.

59

60 **Significance statement**

61 An effective threat anticipation system is crucial to survival across species. Natural threats,
62 however, are diverse and have distinct features. To be able to adapt to different modes of
63 danger, the brain needs to recognize these features, integrate them and use them to modify
64 behavior. Our results disclose the human anterior hippocampus as a likely arbiter of
65 approach/avoidance decisions harnessing compound environmental information while
66 partially replicating previous findings and blending into recent efforts to illuminate the neural
67 basis of approach-avoidance conflict in humans.

68

69

70 **Introduction**

71

72 Integrating divergent situational demands is critical to survival; in particular when predatory
73 or metabolic threat is involved (Korn and Bach, 2015, 2018, 2019). A standard laboratory
74 model of this situation is provided by approach-avoidance conflict (AAC) tests, e.g. open-field
75 test and elevated plus-maze (Calhoun and Tye, 2015), which are thought to reflect aspects
76 of human clinical anxiety disorders (Aupperle and Paulus, 2010). Situational threat features
77 are manifold and distinct in these tests, and even more so in biological scenarios (Evans et
78 al., 2019). For a human during wintertime, there is a low probability of being attacked when
79 encountering a hibernating bear and a higher probability when coming across wolves, who
80 are short on food. The metabolic loss incurred by a bear chase, however, may be much
81 higher than when being charged by a single wolf. How the neural system represents and
82 integrates such different threat dimensions, and how they influence behavior, e.g., the
83 decision to approach food under threat or passively avoid threat, remains unknown.

84

85 In rodent AAC tests, cautious ("anxiety-like") behavior is consistently reduced by anxiolytic
86 drugs such as benzodiazepines (Gray and McNaughton, 2000). Ventral hippocampus lesions
87 have a similar impact (Kjelstrup et al., 2002; Bannerman et al., 2003; McHugh et al., 2004;
88 Ito and Lee, 2016; Kirlic et al., 2017), and it has been suggested that behavioral control
89 requires interplay of hippocampal subfields (Schumacher et al., 2018). Theta oscillations of
90 hippocampal local field potential (Gordon et al., 2005), and synchronization with prefrontal
91 cortex (Adhikari et al., 2010; Padilla-Coreano et al., 2016), are increased in AAC, while area-
92 specific circuits influence decisions (Wallis et al., 2019). In a human computer game
93 resembling open-field test, benzodiazepines (Korn et al., 2017) and other anxiolytics (Bach et
94 al., 2018) reduced cautious behavior similar to hippocampus (Bach et al., 2014) and
95 amygdala (Korn et al., 2017) lesions in humans and non-human primates (Chudasama et al.,
96 2008; Machado et al., 2009). Amygdala contribution is inconsistently reported in rodents
97 (Kirlic et al., 2017); in humans it appears to be specifically required for retreat from threat
98 after reward collection, rather than for the decision to approach (Bach et al., 2019).

99

100 While this suggests involvement of hippocampus and amygdala in behavioral control, it
101 remains elusive how different threat features, ultimately determining behavior, are
102 represented and integrated. Features such as magnitude and probability of threat are not
103 experimentally controlled in many tests that build on innate anxiety, or that are extended in
104 time. For example, we have shown using functional magnetic resonance imaging (fMRI) that
105 neural mass activity of anterior hippocampus (aHC) increases with threat probability in
106 continuous-time AAC (Bach et al., 2014). However, fMRI studies with more abstract AAC

107 tests not requiring immediate behavior have yielded conflicting results, some suggesting the
108 same relation of aHC activity with threat probability (Korn and Bach, 2019); others a relation
109 of aHC activity (Loh et al., 2017) or multivoxel patterns (O'Neil et al., 2015) with behavior.

110

111 Operant conflict tests provide the opportunity to more precisely control threat features as
112 demonstrated in rodents (Evenden et al., 2009; Oberrauch et al., 2019) and humans (Bach,
113 2015, 2017; Bach et al., 2019). Here, we capitalized on this latter operant AAC test to
114 disambiguate representation of attack probability, its metabolic cost, and behavior, in aHC
115 and amygdala. We previously used the same task to show that putative hippocampal gamma
116 oscillations, and hippocampal theta synchronization with prefrontal cortex, increased with
117 threat probability (Khemka et al., 2017). Presently, we gained from the superior spatial
118 resolution of fMRI collecting 1.5 mm isotropic blood-oxygen-level-dependent (BOLD) images
119 focused on amygdala and hippocampus while participants played the game. On each trial,
120 they could either collect, or forgo, a monetary token under threat of capture by a predator.
121 Threat probability was defined by the predator wake-up rate and learned by experience;
122 threat magnitude by potential token loss and explicitly signaled.

123

124

125

126 **Materials and Methods**

127

128 *Participants*

129

130 Twenty participants were recruited from general and student population in Zurich (mean age
131 \pm SD, 23.10 \pm 3.34 years; 11 female). Participants had no prior history of neurological or
132 psychiatric disease and reported normal or corrected-to-normal vision. One participant was
133 excluded from fMRI analysis due to a technical fault in MRI recordings, but included in
134 behavioral analysis. Behavioral results remained consistent after removal of this participant.
135 All participants gave their written informed consent before participation. The study protocol
136 was in full accordance with the Declaration of Helsinki and approved by the governmental
137 ethics committee (Kantonale Ethikkommission Zürich).

138

139

140 *Experimental procedure*

141

142 Participants performed an AAC computer game as previously used in Khemka et al. (2017),
143 which was modified from Bach (2015). At the beginning of each trial, the human player was

144 located in a "safe place" in the bottom block of a 2 x 2 diamond grid (Fig 1) opposite of a
145 sleeping predator, and was given the opportunity to collect a monetary token that would
146 appear in the left or right grid block. Red diamonds underneath the grid explicitly signaled
147 the number of tokens that would be lost (0-5) if captured by the predator. Threat probability
148 was implicitly signaled through frame color (blue, pink and orange). Threat probability was
149 implemented by setting the wake-up rate per time unit to result in catch probabilities of 0.1,
150 0.2, or 0.3 per 100 ms spent outside of the safe grid block. These probabilities were learned
151 from experience during 36 preceding training trials without token loss that did not count
152 towards ultimate earnings.

153 A token appeared after a random time interval drawn from a truncated gamma distribution (k
154 $= 2$, $\theta = 1$; mean = 2 s, $t \leq 6$ s). If the player chose not to collect the token, it would disappear
155 after another time interval drawn from the same distribution, and the trial would end one
156 second later. If the player went to acquire the token and successfully returned to the safe
157 place, the trial would proceed until the same predetermined end time. Finally, if the predator
158 caught the player, the predator changed its color from gray to red and remained on the
159 screen until the predetermined end time of the trial. After a random intertrial interval (ITI) also
160 drawn from a gamma distribution truncated at $t \leq 4$ s, during which a blank screen was
161 presented, the next trial would start. Participants completed 648 trials in random order,
162 balanced for each combination of experimental factors, i.e. threat magnitude, and threat
163 probability. Participants were instructed beforehand that their payment depended on
164 performance in six trials randomly drawn from the experiment excluding training trials. The
165 experiment was programmed in Cogent (Version 2000v1.25; www.vislab.ucl.ac.uk/Cogent)
166 and MATLAB (Version 7.14; MathWorks).

167

168

169 *Acquisition of MRI data*

170

171 Data was recorded in a 3.0-Tesla MRI scanner (Phillips Achieva; Phillips Medical Systems,
172 Best Netherlands) using a 32-channel head coil. Anatomical images were acquired using a
173 0.76 mm isotropic resolution T1-weighted scan (TR = 7.37 ms, TE = 3.29 ms, flip angle = 8°,
174 field of view (FOV) = 255x255x180 mm, matrix = 336x336, thickness = 0.76 mm, in-plane
175 resolution = 0.76 x 0.76 mm², slice tilt = 0°, 237 sagittal slices) and a 1.0 x 0.5 x 0.5 mm
176 resolution T2-weighted scan centered on hippocampus (TR = 3200 ms, TE = 353 ms, flip
177 angle = 90°, FOV = 200x52x200 mm, matrix = 400x400, thickness = 1 mm, in-plane
178 resolution = 0.5 x 0.5 mm², slice tilt = 22°, 104 transverse slices). B0 Field maps were
179 acquired with a double-echo fast gradient echo sequence (TR = 698.22 ms, TE = 4.10 and
180 7.10, flip angle = 44°, FOV = 240x224x240 mm, matrix = 80 x 80, thickness = 3 mm, in-plane

181 resolution = $3 \times 3 \text{ mm}^2$, slice tilt = 0° , 2x64 sagittal slices). Functional images during the
182 approach-avoidance paradigm were recorded with 1.5 mm isotropic resolution T2*-weighted
183 echo-planar imaging (EPI) sequence (TR = 2800 ms, TE = 30 ms, flip angle = 85° , in-plane
184 resolution = $1.5 \times 1.5 \text{ mm}^2$, FOV = 216x54x216 mm, matrix = 144x144; 36 transverse slices
185 with thickness = 1.5 mm; slice order = interleaved ascending; slice tilt = -40°). Field of view
186 (FOV) was centered on amygdala/hippocampus, but also encompassed striatum, thalamus,
187 prefrontal cortices with exclusion of orbitofrontal cortex and cranio-posterior segments of
188 frontal lobe, greater parts of temporal lobes and cerebellum as well as complete coverage of
189 insular cortices and brainstem (Fig 1).

190

191

192 *Preprocessing of MRI data*

193

194 Preprocessing of functional images was performed using a standard pipeline in SPM12
195 (Statistical Parametric Mapping; Wellcome Centre for Human Neuroimaging, London, UK;
196 <http://www.fil.ion.ucl.ac.uk/spm/software/spm12>). In a first step, slice time correction was
197 performed to account for differences in acquisition time of individual brain slices (Sladky et
198 al., 2011). Geometric distortions due to susceptibility-induced field inhomogeneities were
199 addressed using a combined approach, which takes static distortions as well as changes in
200 distortion due to head motion into account (Andersson et al., 2001; Hutton et al., 2002).
201 Static distortions were derived for each subject individually from a B0 field map using the
202 FieldMap toolbox in SPM12. Echo-planar images were subsequently realigned and
203 unwarped integrating the measured static distortion and the estimation of distortion caused
204 by head motion, as well as head motion itself. EPI-images as well as T2w-images were then
205 coregistered to the individual T1w whole brain image using a 12-parameter affine
206 transformation. Finally, EPI-images were normalized into Montreal Neurological Institute
207 (MNI) space and smoothed using an isotropic 8 mm full-width at half maximum (FWHM)
208 Gaussian kernel for primary mass-univariate analysis, and a 4 mm FWHM Gaussian kernel
209 for a secondary analysis to improve localization of effects in amygdala and hippocampus. We
210 note that the smoothing kernel must strike a balance between anatomical intersubject
211 variability, and regional specificity (Mikl et al., 2008). Thus, the larger smoothing kernel is
212 expected to be more sensitive in detecting activations, but the smaller kernel can provide
213 additional information on the localization of clusters. Unsmoothed EPI images in native space
214 were used for region-of-interest (ROI) analysis.

215

216

217

218 *fMRI analysis (focused brain coverage)*

219

220 In a primary analysis (P1), we defined a general linear model consisting of a delta function at
221 token appearance (consistent with Khemka et al. 2017), convolved with a canonical
222 hemodynamic response function (HRF). Parametric modulators for linear and quadratic
223 effect of threat probability (1-3), linear and quadratic effect of threat magnitude (0-5), and
224 linear interaction effect of threat probability x magnitude, were also convolved with the HRF.
225 All parametric modulators were serially orthogonalized. Motion correction parameters were
226 included as six additional regressors of no interest.

227 To distinguish effects of behavior from threat features, we ran a second parametric analysis
228 (P2) with approach or avoidance as a first parametric modulator, followed by linear and
229 quadratic effect of threat probability, linear and quadratic effect of threat magnitude, linear
230 combination of threat probability x magnitude, linear combinations of approach x probability,
231 approach x magnitude and finally approach x probability x magnitude.

232 To extricate effects of threat probability and magnitude that were specific to ensuing
233 behavior, we computed a third general linear model with separate trial regressors for
234 approach trials and avoidance trials (P3), each with parametric modulators for linear and
235 quadratic effects of threat probability and magnitude as well as for effect of linear
236 combination of probability x magnitude. To assess a potential relation of neural activity with
237 response latencies, we defined three further models in an analogous manner with parametric
238 regressors for linear and quadratic effects of approach and withdrawal latency during
239 approach trials. We controlled for threat features in all models using serial orthogonalization.
240 Since the player was often caught by the predator during attempts to obtain a token, data for
241 withdrawal latency was available on fewer trials than for approach latency. Thus, we defined
242 one model for approach latency over all trials without control for withdrawal latency, and two
243 models over trials without capture, where approach and withdrawal latencies were
244 orthogonalized in respect to each other.

245

246

247 *Region-of-interest definition*

248

249 Subcortical and cortical structures including hippocampus and amygdala were identified in
250 native subject space using the "recon-all" pipeline in FreeSurfer Version 6.0
251 (<http://surfer.nmr.mgh.harvard.edu/>) (Dale et al., 1999; Fischl et al., 1999a; Fischl et al.,
252 1999b; Fischl et al., 2002; Segonne et al., 2005; Desikan et al., 2006; Fischl et al., 2008).
253 Individual voxels were assigned neuroanatomical labels in an automated volumetric
254 subcortical parcellation based on a probabilistic atlas from a manual training set (Fischl et al.,

255 2002). The hippocampus segmentation was then further parcellated into anterior and mid-to-
256 posterior hippocampus by automatically splitting the mask at one-third length along the
257 anterior-posterior axis of the image in MATLAB (Strange et al., 2014). For exploratory
258 purposes, CA1 and CA2/3 subfields as well as a mask for dentate gyrus of the hippocampus
259 were obtained from FreeSurfer 6.0, which uses a statistical atlas based on ultra-high
260 resolution ex vivo data and combines T1w- and T2w-images for multispectral segmentation
261 (Iglesias et al., 2015). CA1, CA2/3 and dentate gyrus images were then multiplied with the
262 binary anterior hippocampus mask to focus only on the anterior segments.

263 For small volume correction of group-level analysis, a group-level bilateral hippocampus
264 mask was generated by warping the individual bilateral hippocampus masks into MNI space
265 using the deformation fields acquired during normalization of whole-brain T1w images in
266 SPM12. These were then averaged, thresholded at 0.1 and binarized using the SPM12
267 function `ImCalc`. For visualization, group-level masks in MNI space for all significant clusters
268 were extracted using SPM12 Results.

269

270

271 *Region-of-interest fMRI analysis*

272

273 For analysis of estimated condition-by-condition BOLD response, averaged within regions of
274 interest (ROI), we defined a first-level general linear model with separate regressors for 36
275 possible distinct combinations of threat probability (1-3), magnitude (0-5) and behavioral
276 response (0/1). We extracted estimated condition-by-condition BOLD response for anterior
277 hippocampus, anterior subfields CA1 and CA2/3, anterior dentate gyrus, entire amygdala,
278 centrocortical and basolateral amygdala subnucleus groups, and, for visualization, for
279 significant clusters from focused brain analysis.

280

281

282 *Statistical Analysis*

283

284 Image-based statistical tests for fMRI analysis were performed with SPM group level analysis
285 using cluster-level family-wise error (FWE) correction for multiple comparisons at a voxel-
286 inclusion threshold of $p < 0.001$ (correction for whole field of view, or small volume corrected
287 for hippocampus) and applying a random-field theory based approach as implemented in
288 SPM (Worsley et al., 1992).

289

290 For a priori ROIs amygdala and hippocampus, we implemented a mixed effects analysis in R
291 3.4.3 (www.r-project.org) using function `lmer` (`lme4` package) with the following fixed effects

292 that followed the definition of the voxel-wise analysis while adding a hemispheric difference:
293 linear and quadratic effects of threat probability and magnitude, behavioral response and
294 hemisphere, and ensuing interactions. We added a random intercept for subject. This
295 resulted in the R formula (where all predictors are numerical rather than factors):

296

297 $Y \sim 1 + (\text{threat probability} * \text{threat magnitude} + \text{threat probability}^2 + \text{threat}$
298 $\text{magnitude}^2) * \text{behavioral response} * \text{hemisphere} + (1|\text{subject})$

299

300 Exploratory analysis in anterior hippocampus subfields (CA1, CA2/3) and amygdala
301 subnuclei groups (basolateral and centrocortical) was then performed using the same
302 formula. Significance level α was adjusted for multiple comparisons across two regions of
303 interest for a priori tests, and four regions of interest for exploratory analysis using the Holm-
304 Bonferroni method (Holm, 1979). To further differentiate for region- and subfield-specific
305 effects in an exploratory analysis, ROI was included as a fixed effect in one combined model
306 for amygdala vs. aHC and another for anterior CA1 vs. CA2/3. Lastly, post-hoc ROI analysis
307 was performed in anterior dentate gyrus using the initial model without ROI as factor.

308 Statistical analysis of behavioral data was likewise performed in R using a linear mixed-
309 effects model (lme4 package), which can deal with the inherently unbalanced data (see for
310 details: (Bach, 2015; Khemka et al., 2017)), using Satterthwaite approximation to degrees of
311 freedom to appropriately control the false positive rate (Luke, 2017).

312

313

314 *Data availability*

315

316 A repository of unthresholded SPM activations maps for parametric analyses P1-3 (group-
317 level; 4 and 8 mm kernel) is publicly available [https://github.com/a-abivardi/neural-threat-](https://github.com/a-abivardi/neural-threat-behavior-AAC-fMRI)
318 [behavior-AAC-fMRI](https://github.com/a-abivardi/neural-threat-behavior-AAC-fMRI) (Abivardi et al., 2020).

319

320

321 **Results**

322

323 *Behavioral results*

324

325 We first interrogated whether behavior was comparable to previous findings. Passive
326 avoidance (i.e. the proportion of avoidance over approach decisions) increased with higher
327 threat probability and magnitude. Behavioral inhibition, measured as approach latency,
328 increased with higher threat probability and magnitude, while the opposite pattern was

329 observed for withdrawal latency (Fig 2 / Table 1). These results replicate previous reports
330 (Bach, 2015, 2017; Khemka et al., 2017; Bach et al., 2019) and are in concordance with
331 known behavior from rodent studies.

332

333

334 *Mass-univariate fMRI results*

335

336 As threat features and approach/avoidance behavior are strongly related, we chose a
337 threefold parametric design (P1-3) to disentangle distinct effects using serial
338 orthogonalization as implemented in SPM12. In a primary analysis (P1; Table 2), we
339 analyzed how BOLD signal related to linear and quadratic components of the two threat
340 dimensions and their interactions, by including them as parametric modulators. A second
341 analysis (P2; Table 3) prepended these modulators by behavioral response
342 (approach/avoidance), making use of serial orthogonalization in SPM12, and further
343 examined interactions between threat dimensions and behavior. Lastly (P3; Table 4),
344 approach and avoidance trials were analyzed separately to account for behavior-specific
345 effects of threat dimensions on brain activation. All results were corrected for family-wise
346 error (FWE) within the FOV. For bilateral hippocampus, additional FWE small volume
347 correction was performed using a group-level bihemispheric mask, as we had strong a priori
348 hypotheses for this region. Mass-univariate results are reported for images smoothed with an
349 8 mm Gaussian kernel, unless otherwise specified.

350 In analysis P1, we observed higher BOLD signal with a combination of higher threat
351 probability and higher threat magnitude in left anterior hippocampus (specifically subiculum)
352 and entorhinal cortex (linear x linear interaction, FOV-corrected corrected, Fig 3, Table 2).
353 This effect was not reproduced in a secondary analysis with a narrower smoothing kernel
354 size of 4 mm. There were no mass-univariate effects in the amygdala. Exploratory analysis of
355 the remaining brain coverage (Table 2) revealed higher BOLD signal with lower threat
356 probability (linear negative effect of threat probability) in left dorsolateral prefrontal cortex
357 (dlPFC), a cluster extending into left putamen and anterior insula, and in the posterior lobe of
358 the right cerebellum. Low threat magnitude was related to higher BOLD signal (linear
359 negative effect of threat magnitude) in left internal capsule/putamen, posterior short gyrus of
360 left insula, ventrolateral PFC (vlPFC), left inferior temporal gyrus and multiple clusters in
361 bilateral cerebellum and vermis.

362 In P2, there were no significant hippocampus or amygdala clusters at FOV correction. After
363 small volume correction (SVC) in bilateral hippocampus, we observed a cluster in which
364 avoidance behavior related to higher BOLD activity. This cluster in left anterior hippocampus

365 (subiculum) and entorhinal cortex was located slightly posterior to the area modulated by
366 combined threat magnitude and probability in P1 (Fig 3, Table 3). This result was replicated
367 in a secondary analysis using 4 mm kernel smoothed images for higher localization
368 accuracy. In this analysis, the cluster was in adjacent location, but more superior in the
369 anterior CA3/dentate gyrus area (Fig 3). In a distinct cluster in left middle hippocampus (8
370 mm kernel only), high BOLD signal related to high threat magnitude. Exploratory analysis of
371 the remaining brain coverage (Table 3) revealed that approach behavior related to BOLD
372 signal in two large clusters encompassing bilateral cerebellum and extending from bilateral
373 thalamus to striatum and midbrain structures. Furthermore, approach behavior related to
374 activation in left substantia nigra, bilateral anterior cingulate cortex and dorsomedial PFC
375 (dmPFC), anterior short gyrus of right insula, opercular part of right inferior frontal gyrus and
376 precentral cortex. These clusters showed partial overlap with impact of low threat magnitude
377 as shown in P1, in bilateral cerebellum, left putamen and anterior insula, as well as with
378 impact of low threat probability in right cerebellum and left putamen. After controlling for
379 behavior in P2, no linear effects of threat probability were observed. A quadratic modulating
380 effect of threat probability emerged in the left lateral amygdaloid nucleus (8 mm kernel only),
381 i.e. high activation for low and for high, but not for medium threat probability (Fig 3). High
382 threat magnitude was related to high BOLD signal in right anterior insula (anterior and middle
383 short gyrus) and frontal operculum. A second adjacent cluster in the right frontal operculum
384 showed a linear relation of BOLD signal with threat magnitude specifically in combination
385 with approach (interaction threat magnitude x behavior). This effect, however, was only
386 estimable in 16 subjects.

387 In P3, there were no hippocampus or amygdala clusters at whole-brain or small-volume
388 correction. Exploratory analysis of the remaining brain coverage (Table 4) revealed that for
389 approach trials, high threat magnitude was associated with high BOLD signal in bilateral
390 anterior short gyrus of insula, opercular part of inferior frontal gyrus and bilateral anterior
391 cingulate. Overlap with activation related to approach behavior in P2 was seen primarily in
392 anterior cingulate while overlap with activation related to high threat magnitude in P2 was
393 seen in right anterior insula (replicating the previous finding). Linear interaction of high threat
394 probability and magnitude in approach trials (estimable in 17 subjects) furthermore related to
395 BOLD signal in right superior colliculus (partial overlap with approach related activation from
396 P2) and a cluster extending from left brachium of inferior colliculus into the medial geniculate
397 nucleus. Specifically, BOLD response increased with threat magnitude for medium and high
398 threat probabilities, but not for low probability.

399 Effects in avoidance trials were only partially estimable due to unequal distribution (i.e.
400 relative scarcity of avoidance trials across participants) and yielded no significant results.

401 Finally, we found a positive relation of approach latency with BOLD activation in left anterior
402 cingulate cortex and right anterior insula over all approach trials. When controlling for
403 withdrawal latency in the subset of trials where the player was not caught, neither this nor
404 any other relation was seen. There were no significant clusters in relation to withdrawal
405 latency independent of approach latency or threat features.

406

407 *Region-of-interest analysis results*

408 A priori ROI analysis was carried out across both anterior hippocampi, and across both
409 amygdalae. Results were corrected for multiple comparisons across the two ROIs using
410 Holm-Bonferroni adjusted significance level (Table 5).

411 In the anterior hippocampus ROI, we observed a linear main effect of behavioral response
412 and quadratic main effects for threat probability and magnitude. BOLD signal was higher for
413 avoidance than for approach trials. Similar to left lateral amygdala in parametric analysis P2,
414 anterior hippocampus also responded to low and high threat probability (positive quadratic
415 effect). Strikingly, this effect seemed to be behavior-dependent and lateralized as left anterior
416 hippocampus responded to high threat probability and right hippocampus activation related
417 to low threat probability; both during avoidance only (quadratic x linear interaction of threat
418 probability and behavior, and linear interaction of threat probability x behavior x hemisphere)
419 (Fig 4). Moreover, for zero threat magnitude, hippocampus BOLD signal was low, while
420 increasing to peak levels for low to intermediate levels and falling again with higher
421 magnitude, resulting in a significant negative quadratic pattern. Finally, anterior hippocampus
422 exhibited a complex linear interaction of threat features and hemisphere: BOLD response
423 showed a negative linear relation with threat magnitude for high threat probability and for left
424 hemisphere only.

425 The response to low and high threat probability seen in lateral amygdala after control for
426 behavior was replicated in the amygdala ROI analysis (positive quadratic main effect), while
427 interactions between threat probability and behavior were not detected. Left hemisphere
428 showed overall higher BOLD responses in the amygdala.

429 A combined analysis of amygdala and anterior hippocampus revealed distinct activation
430 patterns in relation to behavior (Fig 4 / Table 5). While aHC was clearly more active during
431 avoidant behavior amygdala exhibited a slightly higher BOLD response during approach
432 (behavior x ROI interaction). The quadratic response to threat magnitude appeared to be
433 specific to aHC; moreover aHC was different from amygdala in its lateralized response to
434 threat probability during avoidance (linear threat probability x magnitude x behavior x ROI

435 interaction).

436 In addition to planned ROI analysis, exploratory follow-up analyses were carried out in
437 bilateral anterior hippocampus subfields CA1 and combined CA2/3 as well as basolateral
438 and centrocortical amygdala ROIs. Results were corrected for multiple comparisons across
439 four ROIs using Holm-Bonferroni method (Table 5).

440 Subfield analysis in anterior CA1 revealed complex and interacting effects of threat
441 dimensions with distinct activation patterns for approach and avoidant behavior and
442 depending on hemisphere. As in entire aHC, a relation to low and high threat probabilities
443 was seen during avoidance only (quadratic x linear interaction). A complex linear interaction
444 effect of threat features and hemisphere also similar to entire aHC was observed.

445 Activation in combined hippocampal subfield CA2/3 was higher for avoidance than approach
446 behavior, reflecting the main effect found in the combined anterior hippocampus ROI. The
447 difference (or increase) in BOLD response for avoidance compared to approach conditions,
448 was furthermore higher for anterior CA2/3 ($M=1.31$, $SD=1.28$) than for subfield CA1 ($M=0.22$,
449 $SD=1.17$) in a post-hoc paired sample t-test ($t(17) = -3.31$, $p = 0.004$), underlining the
450 difference between the two subfields. A combined model for the subfields confirmed this
451 distinction with a significant behavior x ROI interaction effect (Fig 4 / Table 5). At the
452 suggestion of a reviewer, we analyzed BOLD responses in anterior dentate gyrus, based on
453 findings that this area may have a role similar to that of CA3. However, we did not find a
454 significant relation with avoidant behavior here.

455

456 Further exploratory analysis in amygdala subnuclei using a probabilistic amygdala mask from
457 a previous study (Abivardi and Bach, 2017) revealed activation of basolateral amygdala with
458 increasing threat magnitude (linear main effect). This effect was not seen for entire
459 amygdala. Left basolateral and centrocortical amygdala were more active than amygdala of
460 the right hemisphere as also seen for entire amygdala. Also, centrocortical amygdala
461 exhibited heightened BOLD response to intermediate threat magnitudes, especially during
462 avoidance (quadratic main effect + quadratic x linear interaction). We note that the
463 centrocortical amygdala parcellation was defined by structural connectivity with lateral
464 orbitofrontal cortex (Bach et al., 2011) based on preferred projections to central, medial and
465 cortical amygdala in rodents and non-human primates (Carmichael and Price, 1995;
466 McDonald, 1998; Pitkänen, 2000). Morphologically, this group parcellation (resulting from a
467 sample with size of $n=50$; (Abivardi and Bach, 2017) probably includes central, medial,
468 cortical, as well as basomedial nuclei.

469

470 **Discussion**

471 Rodent and human ventral or anterior hippocampus are crucial to cautious behavior in AAC
472 tests (Ito and Lee, 2016). However how distinct threat features are represented and
473 integrated has only recently received attention (Korn and Bach, 2019). Harnessing a human
474 operant AAC computer game during high-resolution fMRI, we investigated representation of
475 threat probability and threat magnitude, and of approach or avoidance behavior, in anterior
476 hippocampus (aHC) and amygdala. Two key findings emerged. First, aHC BOLD activity was
477 related to behavioral avoidance, particularly for CA2/3 but not for CA1. Secondly, there was
478 no evidence that aHC unambiguously represents elementary threat features in a linear
479 manner. Similarly, exploratory analyses of further brain areas within our limited coverage did
480 not reveal a coherent linear representation of threat probability or magnitude.

481
482 In mass-univariate analysis we observed that BOLD signal in left aHC/entorhinal cortex,
483 specifically the subiculum-entorhinal area, was related to the combination of high probability
484 and magnitude of threat (analysis P1), both of which result in more avoidant behavior. After
485 controlling for behavior (P2), no such relation was found. Instead, neural activity in a slightly
486 more posterior cluster was related to avoidant behavior. Using a smaller smoothing kernel to
487 fully harness high spatial resolution, we localized this second cluster to the anterior
488 CA3/dentate gyrus area. A priori ROI analysis confirmed these findings: averaged aHC
489 BOLD signal was increased during avoidance. Follow-up analysis of anterior subfields
490 revealed that this avoidance-related increase occurred in CA2/3 but not CA1. This finding
491 resonates with a rat experiment by Schumacher et al. (2018) who demonstrated that
492 selective pharmacological inactivation of ventral CA3 increased approach behavior. A role
493 paralleling CA3 has been recently described for rodent ventral dentate gyrus (Yeates et al.,
494 2019). We note that it remains possible that our CA2/3 parcellations contain individual voxels
495 belonging to bordering dentate gyrus. Nonetheless, exploratory ROI analysis in dentate
496 gyrus did not detect a similar effect here. On the other hand, CA1 activity in our study
497 showed no simple relationship with threat features or behavior, whereas selective
498 pharmacological ventral CA1 inactivation increased avoidance in a previous rat experiment
499 (Schumacher et al., 2018).

500
501 Our finding of aHC activity relating to avoidance are in keeping with a previous human fMRI
502 study involving abstract AAC decisions, which reported inferior aHC BOLD activity during
503 avoidance (Loh et al., 2017), in proximity to the left aHC cluster relating to avoidance here.
504 We note that in this previous study, most voxels in this cluster were labeled as belonging to
505 CA1; however, the authors noted that anatomical specificity might have been limited due to
506 lower spatial resolution (3 mm), as opposed to the present approach.

507

508 In a lesion study with the same paradigm as used here, we found that hippocampus lesions
509 impaired approach-avoidance decisions, whereas impact of threat on other behaviors
510 remained intact (Bach et al., 2019), further suggesting a specific role of aHC in generating
511 avoidance behavior. Selective amygdala and hippocampus lesions were moreover
512 associated with shorter approach latency, but not with a different relationship between threat
513 and approach latency. This may suggest that these regions do not contribute to parametric
514 variation in approach latency. In keeping with this, we presently found that variation in
515 approach latency did not relate to hippocampus or amygdala signal. A previous
516 magnetoencephalography study reported a relation between approach latency and posterior
517 hippocampus activity (Khemka et al., 2017), not observed here.

518

519 Regarding threat feature representation, ROI analysis revealed a more complicated picture
520 than previously assumed. Though we observed significant responses of aHC to low and
521 intermediate threat magnitude levels, forming a quadratic pattern, BOLD signal also
522 depended on interactions between threat features and behavior, with some effects strikingly
523 different between hemispheres. Specifically, left aHC responded to high threat probability
524 while right aHC related to low probability during avoidance. In humans, left hippocampus has
525 been implicated in contextual and spatial memory encoding while right hippocampus has
526 been linked to navigation accuracy (Maguire et al., 1998; Spiers et al., 2001). Hemisphere-
527 specific connectivity profiles in human aHC (Robinson et al., 2016) and task-related activity
528 in rat ventral HC (Sakaguchi and Sakurai, 2017) have been reported. However, we note the
529 historical and ongoing debate on lateralization of emotional functions, which is based on
530 partly contradicting observations (Gainotti, 2019). It would therefore appear useful to
531 replicate our findings in an independent sample.

532

533 In contrast, a previous fMRI study (Bach et al., 2014) using a more ethological paradigm
534 reported linearly increasing activity in left aHC with higher threat probability. Accounting for
535 the influence of behavior in this temporally extended paradigm was, however, difficult.
536 Furthermore, previous threat probabilities were higher (0.2/0.5/0.8) than the current ones
537 (0.1/0.2/0.3). Also, this previous study did not explicitly control threat magnitude, which we
538 achieved here. Another fMRI study involving more abstract foraging decisions under
539 predation (Korn and Bach, 2019) found a cluster in which aHC signal increased with threat
540 probability (0.1-0.4) but a partly overlapping cluster in which aHC signal decreased from 0.1-
541 0.3 and increased from 0.3-0.4, yielding an overall quadratic pattern. To reconcile these
542 findings, it appears necessary to cover a larger probability range.

543

544 As a further finding, BOLD signal in left lateral amygdala related to low and high, but not
545 intermediate threat probability independent of behavior (P2). ROI analysis in entire amygdala
546 exhibited replicated this behavior-independent activation pattern. The role of amygdala in
547 AAC is reported more controversially than for aHC (Kirlic et al., 2017); nevertheless a recent
548 human lesion study suggested specific involvement in controlling vigor of return to safety
549 (Bach et al., 2019).

550

551 Results from exploratory focused brain analysis revealed several clusters with complex and
552 differential relation with threat features and behavior. Left dorsolateral PFC (dlPFC) response
553 was related to low threat probability (P1), resonating with reports that anxiety is inversely
554 correlated with dlPFC activity (Balderston et al., 2017). Right ventrolateral PFC (vlPFC) has
555 been implicated in motor inhibition and characterized as a "brake", which however has been
556 debated (Aron et al., 2004, 2014; Swick and Chatham, 2014). Here, right vlPFC activity
557 related to low threat magnitude (P1), approach behavior (P2), and high magnitude during
558 approach (P3). While we did observe behavioral inhibition during approach trials relating to
559 threat, the relation to approach behavior seems at odds with pure motor inhibition. Swick and
560 Chatham (2014) propose that vlPFC monitors action-relevant situational changes,
561 compatible with response to threat magnitude here.

562 In a recent optogenetic study, anterior cingulate cortex activation decreased rodent freezing
563 behavior via input to basolateral amygdala (Jhang et al., 2018). Anterior cingulate also
564 appears to signal value predictions of rewards and punishments (Monosov, 2017).
565 Conceptually, dorsal anterior cingulate has been theorized to monitor conflict (or expected
566 value of top-down control) (Botvinick et al., 1999; Shenhav et al., 2016) or to adaptively track
567 context-relevant and action-guiding variables. (Heilbronner and Hayden, 2016). Here, dorsal
568 anterior cingulate related to approach behavior (P2) while also relating to rises in threat
569 magnitude during approach trials (P3). The former finding matches anterior cingulate role in
570 freezing in mice and supports a more active role arbitrating behavior. The latter finding may
571 equally well constitute measurement of conflict, context-relevant variable tracking or
572 punishment-related value predictions.

573

574 Anterior insular cortex activity was related to approach decisions and both threat features.
575 Left insula related to low threat magnitude and probability before accounting for behavior
576 (P1), right anterior insula activation was related to approach (P2) and bilateral insula to high
577 threat magnitude in separated approach trials (P3). This contrasts reports from a study
578 implicating anterior insula activation in avoidance decisions (Aupperle et al., 2015). Overall,
579 insula showed similar responses to anterior cingulate; adding to evidence of their close
580 functional link (Medford and Critchley, 2010).

581

582 Limitations of our study include the use of a limited field-of-view as a necessary compromise
583 for higher resolution imaging of regions-of-interest. Furthermore a relative scarcity of
584 avoidance decisions across participants, compared to previous studies with cumulative token
585 collection (Bach, 2015, 2017; Bach et al., 2019) hindered analysis of threat representation
586 during avoidance and reduced power to detect brain areas involved in avoidant decision-
587 making. A focus on single-stage decisions in the present study precludes analyzing to what
588 extent assumptions about future foraging attempts may prompt avoidance on the current one
589 (Korn and Bach, 2019; Zorowitz et al., 2020). Lastly, orthogonalization in SPM12 penalizes
590 parametric modulators in a serial manner along the design matrix, which demands careful
591 interpretation of results (Mumford et al., 2015).

592

593 To summarize, in this study we disambiguated a relation of neural tissue activity with
594 behavior and situational threat features. Anterior hippocampus BOLD signal, in particular in
595 CA2/3, increased when participants avoided threat. Representation of threat features
596 showed a complicated pattern, and for threat probability depended on behavior. This is in line
597 with a notion that hippocampus does not linearly represent threat features but retrieves them,
598 possibly in a manner that changes over time, in order to compute decisions. It would be
599 useful to increase the range of these threat features, as well as improve both spatial and
600 temporal precision of recording, for example using electrophysiology, to understand how
601 these computations emerge over time in different hippocampal subfields.

602

603

604 **References**

605

- 606 Abivardi A, Bach DR (2017) Deconstructing white matter connectivity of human amygdala
607 nuclei with thalamus and cortex subdivisions in vivo. *Human brain mapping* 38:3927-
608 3940.
- 609 Abivardi A, Khemka S, Bach DR (2020) Hippocampal Representation of Threat Features and
610 Behavior in a Human Approach-Avoidance Conflict Anxiety Task: Unthresholded
611 SPM Activation Maps [Data set]. <https://doi.org/10.5281/zenodo.3893442>.
- 612 Adhikari A, Topiwala MA, Gordon JA (2010) Synchronized activity between the ventral
613 hippocampus and the medial prefrontal cortex during anxiety. *Neuron* 65:257-269.
- 614 Andersson JL, Hutton C, Ashburner J, Turner R, Friston K (2001) Modeling geometric
615 deformations in EPI time series. *Neuroimage* 13:903-919.
- 616 Aron AR, Robbins TW, Poldrack RA (2004) Inhibition and the right inferior frontal cortex.
617 *Trends Cogn Sci* 8:170-177.

- 618 Aron AR, Robbins TW, Poldrack RA (2014) Inhibition and the right inferior frontal cortex: one
619 decade on. *Trends Cogn Sci* 18:177-185.
- 620 Upperle RL, Paulus MP (2010) Neural systems underlying approach and avoidance in
621 anxiety disorders. *Dialogues in clinical neuroscience* 12:517-531.
- 622 Upperle RL, Melrose AJ, Francisco A, Paulus MP, Stein MB (2015) Neural substrates of
623 approach-avoidance conflict decision-making. *Human brain mapping* 36:449-462.
- 624 Bach DR (2015) Anxiety-Like Behavioural Inhibition Is Normative under Environmental
625 Threat-Reward Correlations. *PLoS Comput Biol* 11:e1004646.
- 626 Bach DR (2017) The cognitive architecture of anxiety-like behavioral inhibition. *J Exp*
627 *Psychol Hum Percept Perform* 43:18-29.
- 628 Bach DR, Korn CW, Vunder J, Bantel A (2018) Effect of valproate and pregabalin on human
629 anxiety-like behaviour in a randomised controlled trial. *Transl Psychiatry* 8:157.
- 630 Bach DR, Behrens TE, Garrido L, Weiskopf N, Dolan RJ (2011) Deep and superficial
631 amygdala nuclei projections revealed in vivo by probabilistic tractography. *J Neurosci*
632 31:618-623.
- 633 Bach DR, Hoffmann M, Finke C, Hurlmann R, Ploner CJ (2019) Disentangling hippocampal
634 and amygdala contribution to human anxiety-like behaviour. *The Journal of*
635 *Neuroscience*:0412-0419.
- 636 Bach DR, Guitart-Masip M, Packard PA, Miro J, Falip M, Fuentemilla L, Dolan RJ (2014)
637 Human hippocampus arbitrates approach-avoidance conflict. *Curr Biol* 24:541-547.
- 638 Balderston NL, Liu J, Roberson-Nay R, Ernst M, Grillon C (2017) The relationship between
639 dIPFC activity during unpredictable threat and CO₂-induced panic symptoms. *Transl*
640 *Psychiatry* 7:1266.
- 641 Bannerman DM, Grubb M, Deacon RM, Yee BK, Feldon J, Rawlins JN (2003) Ventral
642 hippocampal lesions affect anxiety but not spatial learning. *Behav Brain Res* 139:197-
643 213.
- 644 Botvinick M, Nystrom LE, Fissell K, Carter CS, Cohen JD (1999) Conflict monitoring versus
645 selection-for-action in anterior cingulate cortex. *Nature* 402:179-181.
- 646 Calhoun GG, Tye KM (2015) Resolving the neural circuits of anxiety. *Nat Neurosci* 18:1394-
647 1404.
- 648 Carmichael ST, Price JL (1995) Limbic connections of the orbital and medial prefrontal cortex
649 in macaque monkeys. *J Comp Neurol* 363:615-641.
- 650 Chudasama Y, Wright KS, Murray EA (2008) Hippocampal lesions in rhesus monkeys
651 disrupt emotional responses but not reinforcer devaluation effects. *Biol Psychiatry*
652 63:1084-1091.
- 653 Dale AM, Fischl B, Sereno MI (1999) Cortical surface-based analysis. I. Segmentation and
654 surface reconstruction. *Neuroimage* 9:179-194.

- 655 Desikan RS, Segonne F, Fischl B, Quinn BT, Dickerson BC, Blacker D, Buckner RL, Dale
656 AM, Maguire RP, Hyman BT, Albert MS, Killiany RJ (2006) An automated labeling
657 system for subdividing the human cerebral cortex on MRI scans into gyral based
658 regions of interest. *Neuroimage* 31:968-980.
- 659 Evans DA, Stempel AV, Vale R, Branco T (2019) Cognitive Control of Escape Behaviour.
660 *Trends in Cognitive Sciences* 23:334-348.
- 661 Evenden J, Ross L, Jonak G, Zhou J (2009) A novel operant conflict procedure using
662 incrementing shock intensities to assess the anxiolytic and anxiogenic effects of
663 drugs. *Behavioural Pharmacology* 20:226-236.
- 664 Fischl B, Sereno MI, Dale AM (1999a) Cortical surface-based analysis. II: Inflation, flattening,
665 and a surface-based coordinate system. *Neuroimage* 9:195-207.
- 666 Fischl B, Sereno MI, Tootell RB, Dale AM (1999b) High-resolution intersubject averaging and
667 a coordinate system for the cortical surface. *Hum Brain Mapp* 8:272-284.
- 668 Fischl B, Rajendran N, Busa E, Augustinack J, Hinds O, Yeo BT, Mohlberg H, Amunts K,
669 Zilles K (2008) Cortical folding patterns and predicting cytoarchitecture. *Cereb Cortex*
670 18:1973-1980.
- 671 Fischl B, Salat DH, Busa E, Albert M, Dieterich M, Haselgrove C, van der Kouwe A, Killiany
672 R, Kennedy D, Klaveness S, Montillo A, Makris N, Rosen B, Dale AM (2002) Whole
673 brain segmentation: automated labeling of neuroanatomical structures in the human
674 brain. *Neuron* 33:341-355.
- 675 Gainotti G (2019) A historical review of investigations on laterality of emotions in the human
676 brain. *Journal of the history of the neurosciences* 28:23-41.
- 677 Gordon JA, Lacefield CO, Kentros CG, Hen R (2005) State-dependent alterations in
678 hippocampal oscillations in serotonin 1A receptor-deficient mice. *J Neurosci* 25:6509-
679 6519.
- 680 Gray J, McNaughton N (2000) *The Neuropsychology of Anxiety*, Oxford University Press.
681 New York:72-82.
- 682 Heilbronner SR, Hayden BY (2016) Dorsal Anterior Cingulate Cortex: A Bottom-Up View.
683 *Annu Rev Neurosci* 39:149-170.
- 684 Holm S (1979) A Simple Sequentially Rejective Multiple Test Procedure. *Scandinavian*
685 *Journal of Statistics* 6:65-70.
- 686 Hutton C, Bork A, Josephs O, Deichmann R, Ashburner J, Turner R (2002) Image distortion
687 correction in fMRI: A quantitative evaluation. *Neuroimage* 16:217-240.
- 688 Iglesias JE, Augustinack JC, Nguyen K, Player CM, Player A, Wright M, Roy N, Frosch MP,
689 McKee AC, Wald LL, Fischl B, Van Leemput K, Alzheimer's Disease Neuroimaging I
690 (2015) A computational atlas of the hippocampal formation using ex vivo, ultra-high

- 691 resolution MRI: Application to adaptive segmentation of in vivo MRI. *Neuroimage*
692 115:117-137.
- 693 Ito R, Lee AC (2016) The role of the hippocampus in approach-avoidance conflict decision-
694 making: Evidence from rodent and human studies. *Behav Brain Res* 313:345-357.
- 695 Jhang J, Lee H, Kang MS, Lee HS, Park H, Han JH (2018) Anterior cingulate cortex and its
696 input to the basolateral amygdala control innate fear response. *Nat Commun* 9:2744.
- 697 Khemka S, Barnes G, Dolan RJ, Bach DR (2017) Dissecting the Function of Hippocampal
698 Oscillations in a Human Anxiety Model. *J Neurosci* 37:6869-6876.
- 699 Kirlic N, Young J, Aupperle RL (2017) Animal to human translational paradigms relevant for
700 approach avoidance conflict decision making. *Behaviour research and therapy* 96:14-
701 29.
- 702 Kjelstrup KG, Tuvnes FA, Steffenach HA, Murison R, Moser EI, Moser MB (2002) Reduced
703 fear expression after lesions of the ventral hippocampus. *Proc Natl Acad Sci U S A*
704 99:10825-10830.
- 705 Korn CW, Bach DR (2015) Maintaining Homeostasis by Decision-Making. *PLOS*
706 *Computational Biology* 11:e1004301.
- 707 Korn CW, Bach DR (2018) Heuristic and optimal policy computations in the human brain
708 during sequential decision-making. *Nature Communications* 9:325.
- 709 Korn CW, Bach DR (2019) Minimizing threat via heuristic and optimal policies recruits
710 hippocampus and medial prefrontal cortex. *Nature Human Behaviour* 3:733-745.
- 711 Korn CW, Vunder J, Miró J, Fuentemilla L, Hurlemann R, Bach DR (2017) Amygdala Lesions
712 Reduce Anxiety-Like Behavior in a Human Benzodiazepine-Sensitive Approach-
713 Avoidance Conflict Test. *Biological Psychiatry*.
- 714 Loh E, Kurth-Nelson Z, Berron D, Dayan P, Duzel E, Dolan R, Guitart-Masip M (2017)
715 Parsing the Role of the Hippocampus in Approach-Avoidance Conflict. *Cereb Cortex*
716 27:201-215.
- 717 Luke SG (2017) Evaluating significance in linear mixed-effects models in R. *Behavior*
718 *Research Methods* 49:1494-1502.
- 719 Machado CJ, Kazama AM, Bachevalier J (2009) Impact of amygdala, orbital frontal, or
720 hippocampal lesions on threat avoidance and emotional reactivity in nonhuman
721 primates. *Emotion* 9:147-163.
- 722 Maguire EA, Burgess N, Donnett JG, Frackowiak RSJ, Frith CD, Keefe J (1998) Knowing
723 Where and Getting There: A Human Navigation Network. *Science* 280:921.
- 724 Mai JK, Majtanik M, Paxinos G (2016) *Atlas of the human brain*, 4 Edition: Academic Press.
- 725 McDonald AJ (1998) Cortical pathways to the mammalian amygdala. *Prog Neurobiol* 55:257-
726 332.

- 727 McHugh SB, Deacon RM, Rawlins JN, Bannerman DM (2004) Amygdala and ventral
728 hippocampus contribute differentially to mechanisms of fear and anxiety. *Behav*
729 *Neurosci* 118:63-78.
- 730 Medford N, Critchley HD (2010) Conjoint activity of anterior insular and anterior cingulate
731 cortex: awareness and response. *Brain Struct Funct* 214:535-549.
- 732 Mikl M, Mareček R, Hlušík P, Pavlicová M, Drastich A, Chlebus P, Brázdil M, Krupa P (2008)
733 Effects of spatial smoothing on fMRI group inferences. *Magnetic Resonance Imaging*
734 26:490-503.
- 735 Monosov IE (2017) Anterior cingulate is a source of valence-specific information about value
736 and uncertainty. *Nat Commun* 8:134.
- 737 Mumford JA, Poline JB, Poldrack RA (2015) Orthogonalization of regressors in FMRI
738 models. *PLoS One* 10:e0126255.
- 739 O'Neil EB, Newsome RN, Li IH, Thavabalasingam S, Ito R, Lee AC (2015) Examining the
740 Role of the Human Hippocampus in Approach-Avoidance Decision Making Using a
741 Novel Conflict Paradigm and Multivariate Functional Magnetic Resonance Imaging. *J*
742 *Neurosci* 35:15039-15049.
- 743 Oberrauch S, Sigrist H, Sautter E, Gerster S, Bach DR, Pryce CR (2019) Establishing
744 operant conflict tests for the translational study of anxiety in mice.
745 *Psychopharmacology*.
- 746 Padilla-Coreano N, Bolkan SS, Pierce GM, Blackman DR, Hardin WD, Garcia-Garcia AL,
747 Spellman TJ, Gordon JA (2016) Direct Ventral Hippocampal-Prefrontal Input Is
748 Required for Anxiety-Related Neural Activity and Behavior. *Neuron* 89:857-866.
- 749 Pitkänen A (2000) Connectivity of the rat amygdaloid complex. In: *The amygdala: A*
750 *functional analysis* (JP A, ed), pp 31-116. Oxford: Oxford UP.
- 751 Robinson JL, Salibi N, Deshpande G (2016) Functional connectivity of the left and right
752 hippocampi: Evidence for functional lateralization along the long-axis using meta-
753 analytic approaches and ultra-high field functional neuroimaging. *Neuroimage*
754 135:64-78.
- 755 Sakaguchi Y, Sakurai Y (2017) Left–right functional asymmetry of ventral hippocampus
756 depends on aversiveness of situations. *Behavioural Brain Research* 325:25-33.
- 757 Schumacher A, Villaruel FR, Ussling A, Riaz S, Lee AC, Ito R (2018) Ventral hippocampal
758 CA1 and CA3 differentially mediate learned approach-avoidance conflict processing.
759 *Current Biology* 28:1318-1324. e1314.
- 760 Segonne F, Grimson E, Fischl B (2005) A genetic algorithm for the topology correction of
761 cortical surfaces. *Inf Process Med Imaging* 19:393-405.
- 762 Shenhav A, Cohen JD, Botvinick MM (2016) Dorsal anterior cingulate cortex and the value of
763 control. *Nat Neurosci* 19:1286-1291.

- 764 Sladky R, Friston KJ, Trostl J, Cunnington R, Moser E, Windischberger C (2011) Slice-timing
765 effects and their correction in functional MRI. *Neuroimage* 58:588-594.
- 766 Spiers HJ, Burgess N, Maguire EA, Baxendale SA, Hartley T, Thompson PJ, O'Keefe J
767 (2001) Unilateral temporal lobectomy patients show lateralized topographical and
768 episodic memory deficits in a virtual town. *Brain* 124:2476-2489.
- 769 Strange BA, Witter MP, Lein ES, Moser EI (2014) Functional organization of the hippocampal
770 longitudinal axis. *Nat Rev Neurosci* 15:655-669.
- 771 Swick D, Chatham CH (2014) Ten years of inhibition revisited. *Front Hum Neurosci* 8:329.
- 772 Tzourio-Mazoyer N, Landeau B, Papathanassiou D, Crivello F, Etard O, Delcroix N, Mazoyer
773 B, Joliot M (2002) Automated Anatomical Labeling of Activations in SPM Using a
774 Macroscopic Anatomical Parcellation of the MNI MRI Single-Subject Brain.
775 *NeuroImage* 15:273-289.
- 776 Wallis CU, Cockcroft GJ, Cardinal RN, Roberts AC, Clarke HF (2019) Hippocampal
777 Interaction With Area 25, but not Area 32, Regulates Marmoset Approach–Avoidance
778 Behavior. *Cerebral Cortex*.
- 779 Worsley KJ, Evans AC, Marrett S, Neelin P (1992) A three-dimensional statistical analysis for
780 CBF activation studies in human brain. *J Cereb Blood Flow Metab* 12:900-918.
- 781 Yeates DCM, Ussling A, Lee ACH, Ito R (2019) Double dissociation of learned approach–
782 avoidance conflict processing and spatial pattern separation along the dorsoventral
783 axis of the dentate gyrus. *Hippocampus* n/a.
- 784 Zorowitz S, Momennejad I, Daw ND (2020) Anxiety, Avoidance, and Sequential Evaluation.
785 *Computational Psychiatry* 4:1-17.

786

787

788

789

790 **Legends**

791

792

793 **Table 1.** Analysis of Variance (ANOVA) of effects of threat features on behavioral measures
794 with Satterthwaite's approximation. Abbreviations: TP = threat probability, TM = threat
795 magnitude.

796

797 **Table 2.** Parametric modulating effects of threat probability, magnitude and their interaction
798 on brain activation (Analysis P1). FWE-corrected results ($p < .05$) at cluster level (whole-
799 brain + whole-brain/small volume corrected (SVC) for hippocampus), at a voxel-inclusion
800 level inclusion threshold of $p < 0.001$. Manual labeling in comparison with schematic brain
801 atlas (Mai et al., 2016). Automated labeling shows AAL (Tzourio-Mazoyer et al., 2002) peak
802 labels verbatim.

803 **Table 3.** Parametric modulating effects of behavioral response (approach/avoidance),
804 followed by threat probability, magnitude and their interactions on brain activation (Analysis
805 P2). FWE-corrected results ($p < .05$) at cluster level (whole-brain + small volume corrected
806 (SVC) for hippocampus), at a voxel-inclusion level inclusion threshold of $p < 0.001$. Manual
807 labeling in comparison with schematic brain atlas (Mai et al., 2016).

808 **Table 4.** Parametric modulating effects of threat probability, magnitude and their interactions
809 on brain activation in separated approach and avoidance trials (Analysis P3). FWE-corrected
810 results ($p < .05$) at cluster level (whole-brain), at a voxel-inclusion level inclusion threshold of
811 $p < 0.001$. Manual labeling in comparison with schematic brain atlas (Mai et al., 2016).

812 **Table 5.** Main and interaction effects significant after Holm-Bonferroni correction (* $p < 0.05$;
813 ** $p < 0.01$; *** $p < 0.001$) from Analysis of Variance (ANOVA) of mixed effects model of
814 estimated condition-by-condition BOLD response averaged across region-of-interest
815 (entire/subregional amygdala and anterior hippocampus). Significant main and interaction
816 effects from ANOVA of combined mixed effects model for amygdala vs. anterior
817 hippocampus and anterior CA1 vs. anterior C2/3. Abbreviations: TP = threat probability, TM
818 = threat magnitude, A = action, H = hemisphere, ROI = region-of-interest.

819

820 **Figure 1. A:** Field-of-view focused on amygdala/hippocampus. The image shows the EPI
821 coverage across participants (thresholded at $p=.5$), overlaid on a mean T1 image in MNI
822 space. **B:** Approach/avoidance conflict task. In each trial, the human participant (green
823 triangle) started out in a safe (dark gray) grid block opposite a sleeping predator (gray circle)
824 and was presented with a reward token (yellow rhombus) on the left or right side. Threat
825 probability was signaled by frame color (blue/magenta/orange). The player then had the
826 choice to collect the token using left/right keys to move out of, and return to, the safe place. If
827 caught whilst outside, the amount of tokens signaled in red below the frame (here two) was
828 lost, thus constituting the magnitude of threat.

829

830 **Figure 2. A:** Proportion of approach/avoidance decisions \pm SEM defined as SD of
831 generalized linear mixed-effects model residuals divided by square root of number of data
832 points. **B:** Approach and withdrawal latency, estimated from linear mixed-effects model \pm
833 SEM (defined as SD of model residuals divided by square root of number of data points).

834

835 **Figure 3.** Cluster-level significant anterior hippocampus (aHC) and amygdala clusters from
836 parametric analysis with, for purposes of illustration, extracted estimated condition-by-
837 condition BOLD response \pm SEM as defined by SD of BOLD response amplitude estimates
838 divided by square root of number of data points. Primary analysis clusters using 8 mm

839 FWHM smoothing kernel are displayed in red, secondary analysis cluster (B) using 4 mm
840 kernel is overlaid in blue. **A:** Left anterior subiculum-entorhinal cortex cluster modulated by
841 combined threat probability and magnitude (linear positive interaction effect, analysis P1). **B:**
842 Left anterior subiculum-entorhinal cortex area relating to avoidance (P2; small volume
843 corrected). Secondary analysis localized this cluster to the left anterior CA3/dentate gyrus
844 area. BOLD estimates \pm SEM are displayed for the 4 mm cluster. **C:** Left lateral amygdala
845 cluster quadratically modulated by threat probability (P1). All results are FWE corrected at
846 cluster level ($p < .05$; voxel inclusion threshold: $p < .001$).

847 **Figure 4.** Region-of-interest analyses for anterior hippocampus (aHC) (A), amygdala vs.
848 aHC (B) and anterior CA1 vs. anterior CA2/3 (B). **A:** Interaction effect of threat probability,
849 approach and hemisphere: i.e. estimated condition-by-condition BOLD response amplitudes
850 \pm SEM defined as SD of mixed effects model residuals divided by square root of number of
851 data points. **B:** Interaction effect of behavior x ROI for amygdala vs. aHC and anterior CA1
852 vs. anterior CA2/3 (condition-by-condition BOLD response \pm SEM).

Table 1.
 Linear and omnibus effects of threat features on behavioral responses

Action (proportion approach)			Approach latency			
	F	df	p	F	df	p
TP: omnibus	61.36	2, 12923.0	< .001***	12.57	2, 8883.2	< .001***
TP: linear	214.74	1, 12923.0	< .001***	14.14	1, 8883.9	< .001***
TM: omnibus	463.61	5, 12923.0	< .001***	37.59	5, 8884.8	< .001***
TM: linear	1945.61	1, 12923.0	< .001***	173.95	1, 8892.3	< .001***
TP x TM: omnibus	3.58	10, 12923.0	< .001***	3.60	10, 8881.6	< .001***
TP x TM: linear	15.73	1, 12923.0	< .001***	3.52	1, 8883.1	0.061
Withdrawal latency			Movement into correct direction			
	F	df	p	F	df	p
TP: omnibus	13.74	2, 7070.0	< .001***	0.56	2, 8939.0	0.570
TP: linear	18.18	1, 7070.4	< .001***	1.00	1, 8939.0	0.318
TM: omnibus	10.04	5, 7070.5	< .001***	1.53	5, 8939.0	0.176
TM: linear	37.90	1, 7074.0	< .001***	5.57	1, 8939.0	0.018*
TP x TM: omnibus	0.92	10, 7069.1	0.514	0.97	10, 8939.0	0.467
TP x TM: linear	0.80	1, 7069.9	0.371	2.14	1, 8939.0	0.144

Table 2.

Parametric analysis (P1): effects of threat features on brain activation

Cluster anatomy (manual label.)	Cluster size	FWE p-value (cluster level)	Peak z-score	Peak coordinates (MNI - mm)	Peak label (AAL)
Threat probability - negative linear effect					
L middle frontal gyrus [dlPFC]	14	0.049	4.02	-33 45 30	Frontal_Mid_L
L putamen; L insula [anterior short gyrus]	17	0.015	3.97; 3.80	-20 15 -3; -30 18 -8	Putamen_L; Insula_L
R cerebellum	25	0.015	4.23	44 -47 -33	Cerebellum_Crus1_R
Threat magnitude - negative linear effect					
L anterior limb of internal capsule / putamen	36	<0.001	4.41	-23 15 8	Putamen_L
L insula [posterior short gyrus]	16	0.042	4.29	-36 -2 6	NA
R inferior frontal gyrus, opercular part [vIPFC]	16	0.042	4.28	42 9 27	Frontal_Inf_Oper_R
R cerebellum	784	<0.001	4.76	33 -53 -23	Cerebellum_6_R
	82	<0.001	4.50	18 -47 -18	Cerebellum_4_5_R
	56	<0.001	4.30	26 -62 -57	Cerebellum_8_R
	59	<0.001	4.12	9 -72 -26	Cerebellum_6_R
	53	<0.001	4.08	15 -66 -45	Cerebellum_8_R
	34	<0.001	3.92	29 -66 -27	Cerebellum_6_R
L cerebellum	33	<0.001	3.93	-30 -51 -23	Cerebellum_6_L
	16	0.008	3.67	-35 -63 -26	Cerebellum_6_L
Cerebellar vermis	18	0.021	3.76	-3 -59 -32	Vermis_9
L inferior temporal gyrus	17	0.030	3.88	-51 -62 -20	Temporal_Inf_L
Threat probability x magnitude - positive linear effect					
L entorhinal cortex; L pre- and parasubiculum extending into CA1 [of anterior hippocampus]	14	0.043	3.50	-16 -9 -27	ParaHippocampal_L
	12	0.002 (SVC)	3.50; 3.29	-17 -9 -27; -18 -14 -21	ParaHippocampal_L Hippocampus_L

Table 3.

Parametric analysis (P2): effects of approach/avoidance behavior and serially orthogonalized threat features on brain activation

Cluster anatomy (manual labeling)	Cluster size	FWE p-value (cluster)	Peak z-score	Peak coordinates (MNI - mm)	Peak label (AAL)
Effect of approach					
LR Cerebellum	14178	<0.001	6.74; 6.33; 6.00	14 -63 -52; 18 -50 -21; 27 -56 -20	Cerebelum_8_R; Cerebelum_4_5_R; Cerebelum_6_R
LR ventral anterior, mediadorsal and ventral lateral thalamic nuclei; L ventral posterior lateral thalamic nucleus; LR caudate; L putamen; L insula [posterior short gyrus]; L frontal operculum; R habenular nucleus and habenular commissure; periaqueductal grey; R medial geniculate nucleus, L substantia nigra	4677	<0.001	5.50; 5.50; 5.49	-4 -20 12; -15 -15 6; 14 -12 10	Thalamus_L; Thalamus_L; Thalamus_R
R inferior frontal gyrus, opercular part [vIPFC]	220	<0.001	5.03; 4.51; 4.06	58 15 0; 62 14 14; 57 10 8	Frontal_Inf_Oper_R; Frontal_Inf_Oper_R; Frontal_Inf_Oper_R
L substantia nigra	35	<0.001	4.76	-4 -12 -14	NA
LR superior frontal gyrus, medial part [dmPFC / ACC]; LR cingulate gyrus [ACC]	600	<0.001	4.53; 4.51; 4.49	0 42 26; 0 22 32; -4 40 18	Frontal_Sup_Medial_L LCingulum_Mid_L; Cingulum_Ant_L
L cerebellum	40	<0.001	4.41; 3.28	-10 -54 -36; -2 -52 -39	Cerebelum_9_L; Cerebelum_9_L
R insula [anterior short gyrus]	32	<0.001	4.40	42 8 2	Insula_R
R inferior frontal gyrus, opercular part [vIPFC]; R precentral gyrus	187	<0.001	4.24; 4.20; 4.15	48 10 22; 60 10 28; 57 6 20	Frontal_Inf_Oper_R; Precentral_R; Precentral_R
Effect of avoidance					
L pre- and parasubiculum [of anterior hippocampus]/L entorhinal cortex	10 (SVC)	0.012	3.99; 3.81	-20 -20 -21; -24 -21 -20	ParaHippocampal_L; NA
L anterior CA3/dentate gyrus [of anterior hippocampus] (4 mm smoothing kernel)	12 (SVC)	0.039	3.66	-21 -18 -18	

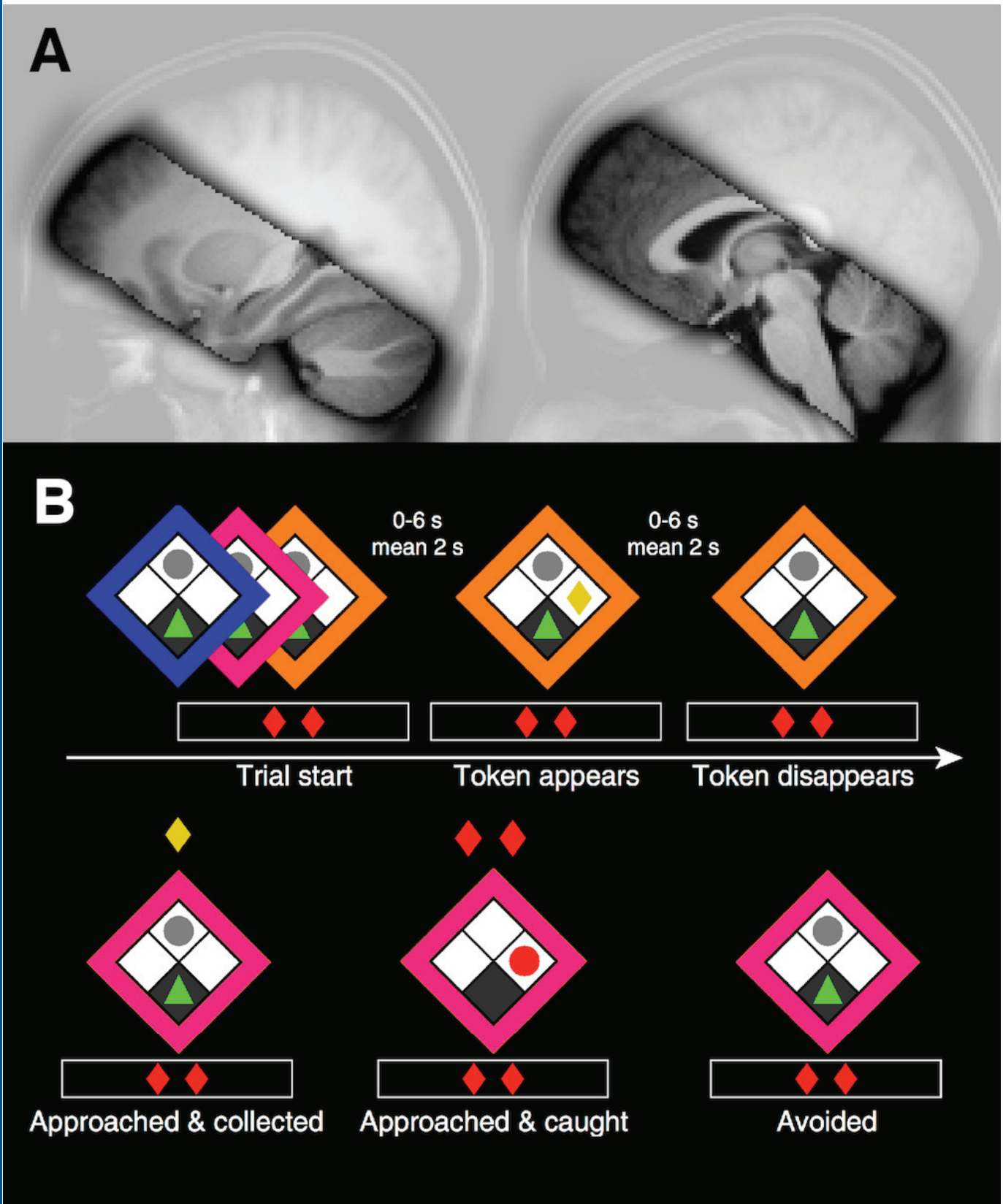
Threat probability - positive quadratic effect (Table 3 cont.)					
L lateral amygdaloid nucleus	25	0.001	4.30	-33 -4 -22	NA
Threat magnitude - positive linear effect					
R insula / area orbitoinsularis [anterior and middle short gyrus]; R frontal operculum, R basal operculum	344	<0.001	4.53; 4.39; 4.29	42 18 -2; 36 21 -10; 51 15 -4	Insula_R; Frontal_Inf_Orb_R; NA
L middle Hippocampus	11	0.004 (SVC)	4.39	-27 -26 -12	Hippocampus_L
Behavioral response x threat magnitude - positive linear effect (n = 16)					
R frontal operculum	21	0.002	3.63	50 20 -3	Frontal_Inf_Oper_R

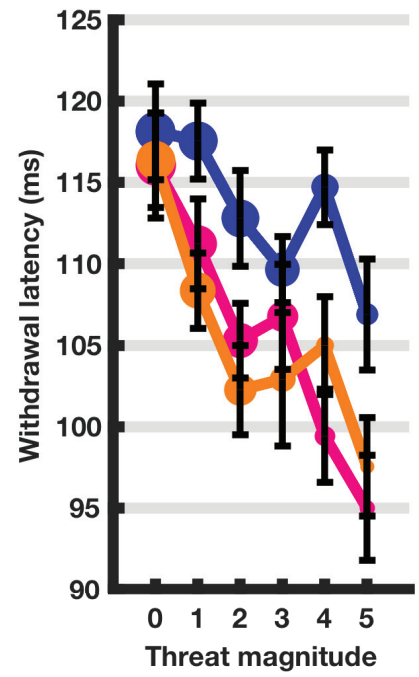
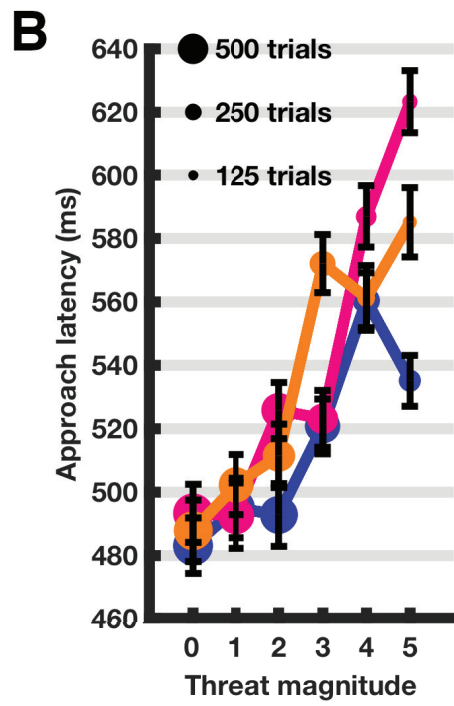
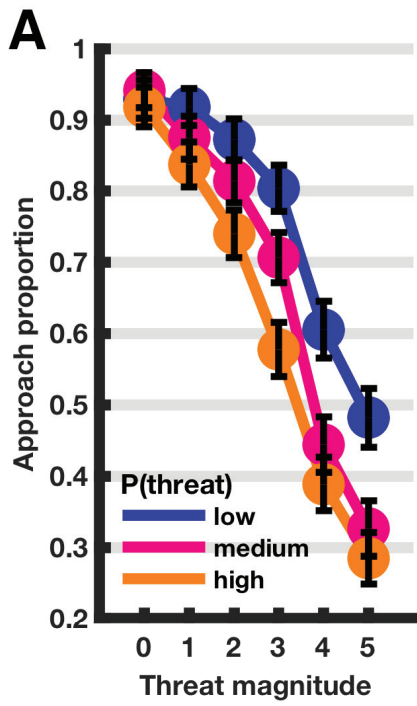
Table 4.
 Parametric analysis (P3): effects of threat features on brain activation, separately for approach and for avoidance trials

Cluster anatomy (manual lab.)	Cluster size	FWE p-value (cluster)	Peak z-score	Peak coordinates (MNI - mm)	Peak label (AAL)
Threat magnitude - positive linear effect (separated approach trials)					
R insula [anterior short gyrus] / R inferior frontal gyrus, opercular part	183	<0.001	4.75; 4.46; 3.66	48 21 -10; 46 18 -3; 42 14 3	Frontal_Inf_Orb_R; Insula_R; Frontal_Inf_Oper_R
L insula [anterior short gyrus] / L inferior frontal gyrus, opercular part	30	0.001	4.26	-46 16 -4	Frontal_Inf_Orb_L
	22	0.012	3.90; 3.82	-39 20 -6; -33 20 2	Insula_L Insula_L
LR superior frontal gyrus, medial part [ACC], LR cingulate gyrus [ACC]	158	<0.001	4.25; 4.23; 4.15	0 27 28; -2 34 26; 6 38 24	Cingulum_Ant_L; Cingulum_Ant_L; Cingulum_Ant_R
	39	<0.001	4.06; 3.79	-2 39 15; 3 44 21	Cingulum_Ant_L; Cingulum_Ant_R
Threat probability x magnitude - linear positive effect (separated approach trials; n = 17)					
L brachium of the inferior colliculus extending into medial geniculate nucleus	19	0.005	4.43	-8 -33 -9	NA
R superior colliculus	20	0.004	4.07	4 -30 -4	NA

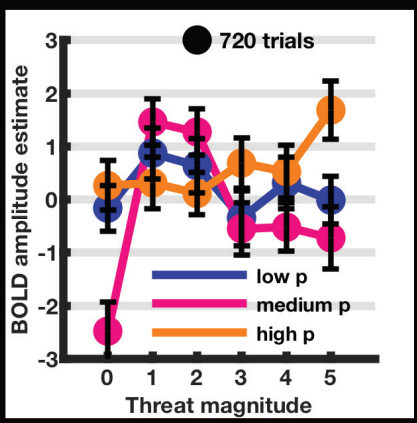
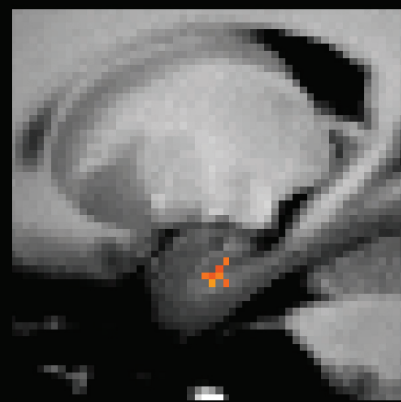
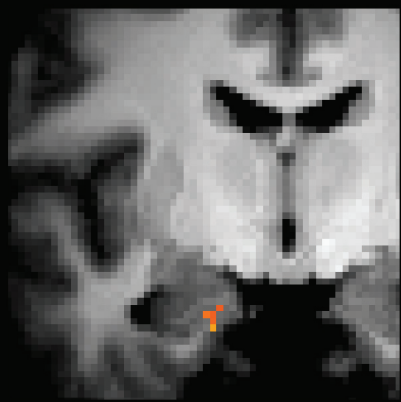
Table 5.
Region-of-interest analyses in anterior hippocampus and amygdala

Anterior Hippocampus			
	F	df	p
A	8.76	1, 1214.6	.003**
TP ²	5.46	1, 1208.2	.020*
TM ²	14.22	1, 1210.1	< .001***
TP x H	5.65	1, 1208.0	.018*
TP ² x A	5.50	1, 1208.9	.019*
TP x TM x H	7.30	1, 1208.0	.007**
TP x A x H	8.38	1, 1208.0	.004**
Amygdala			
H	8.64	1, 1207.9	.003*
TP ²	4.45	1, 1208.2	.035*
Anterior CA1			
TP ² x A	8.88	1, 1208.8	.003**
TP x TM x H	8.65	1, 1208.8	.003**
Anterior CA2/3			
A	10.14	1, 1222.6	.001**
Basolateral Amygdala			
TM	6.26	1, 1210.9	.012*
H	11.13	1, 1207.5	< .001***
Centroccortical Amygdala			
H	6.81	1, 1208.1	.009**
TM ²	9.28	1, 1208.4	.002**
TM ² x A	6.77	1, 1208.1	.009**
Combined model: Anterior Hippocampus + Amygdala			
	F	df	p
A	9.91	1, 2434.9	.002**
ROI	13.61	1, 2433.9	< .001***
TM ²	10.23	1, 2434.2	.001**
TP x H	6.05	1, 2433.9	.014*
A x ROI	7.87	1, 2433.9	.005**
TM ² x ROI	4.98	1, 2433.9	.026*
TP x TM x H	6.82	1, 2433.9	.009**
TP x A x H	8.50	1, 2433.9	.004**
TP x H x ROI	4.39	1, 2433.9	.036*
TP x TM x H x ROI	4.37	1, 2433.9	.037*
TP x A x H x ROI	5.87	1, 2433.9	.015*
Combined model: Anterior CA1 + Anterior CA2/3			
A x ROI	4.95	1, 2670	.026*

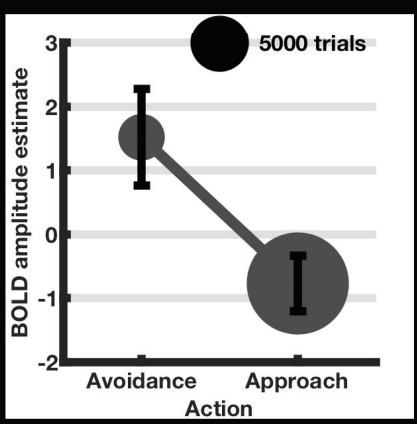
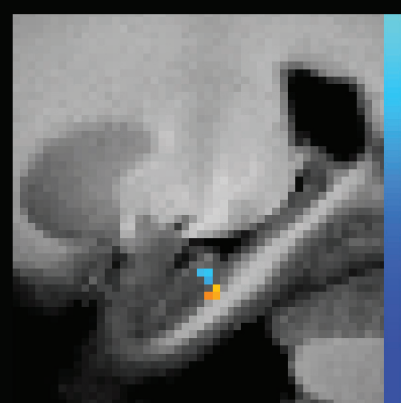
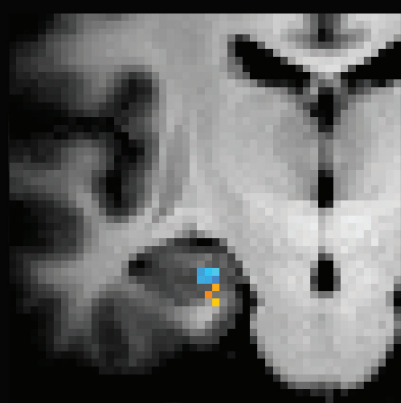




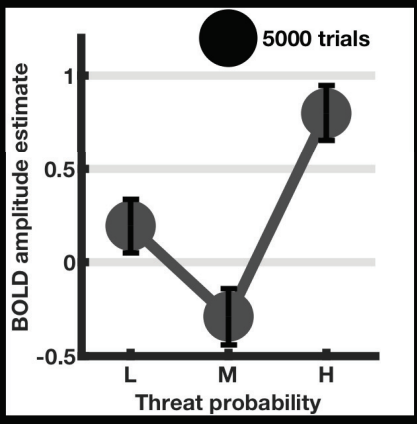
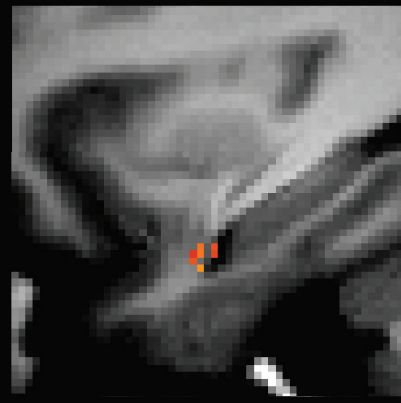
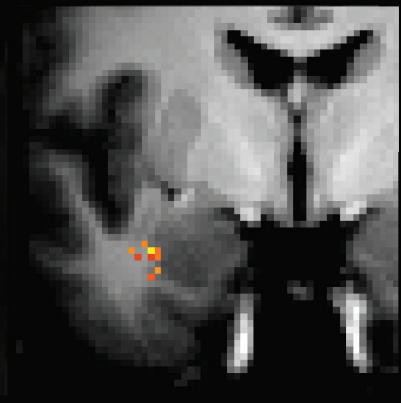
A



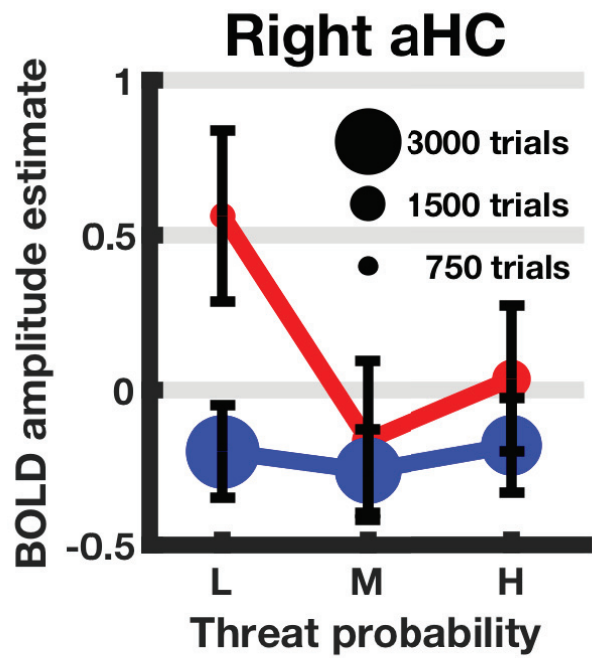
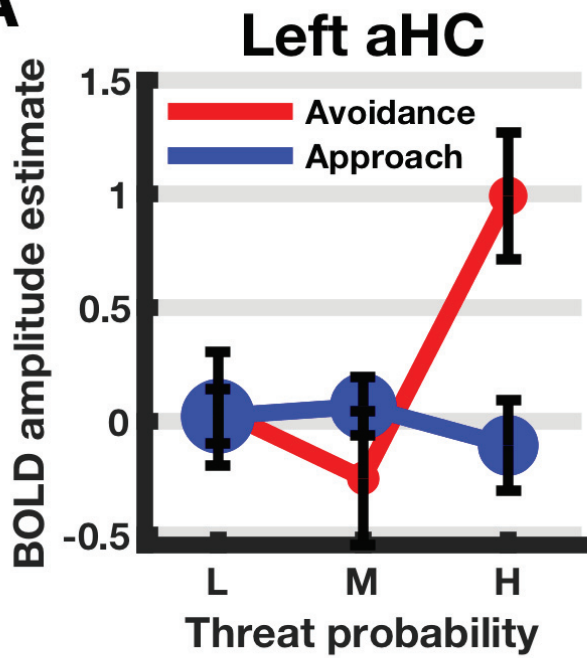
B



C



A



B

